



# Minimizing corner cracking during the de-moulding process of industrial-size GFRP components: a case study

Bryn J. Crawford<sup>1</sup> · Juan Torres<sup>1</sup> · Abbas S. Milani<sup>1</sup>

Received: 21 July 2020 / Accepted: 22 September 2020 / Published online: 3 October 2020  
© Springer-Verlag London Ltd., part of Springer Nature 2020

## Abstract

This article, through an industrial-level case study, presents workflows employed for decision-making to mitigate cracking of glass fibre reinforced polymer (GFRP) parts in tight radii corner locations, often resulting from displacement-controlled de-moulding processes. Namely, using process simulation to evaluate the cure cycle of the GFRP composite parts, it was possible to optimize the time of de-moulding and reduce the potential for part damage. It was observed that the most significant factors influencing the corner defect were boundary conditions of the part during de-moulding, the workshop temperature and part thickness. The poorest process design case was identified as hot workshop temperature, a laminate with thickness on the upper end of tolerances and a boundary condition where most sides are free, allowing for the development of larger moment forces at the tight corners. Further to this, a de-moulding time chart was developed to account for the changes in material properties as a function of temperature and material thickness, allowing for the in situ decision-making of technicians to reduce the occurrence of corner cracks.

**Keywords** Fibre reinforced polymers · Moulding · Part corner cracking · Process characterization · Simulation

## 1 Introduction

Glass fibre reinforced polymers (GFRPs) have become increasingly popular materials of interest in construction, automotive, marine, sporting goods and other manufacturing industries [1, 2]. These cost-efficient composites offer advantages over classical material counterparts, such as metals and pure plastics, by allowing for the manufacture of near-net shape and lightweight parts with complex geometries [3, 4], along with a high-quality, glossy surface finish that can be resistant to corrosive environment during service. However, there are still complexities associated with manufacturing GFRP composite parts, due to the thermo-chemo-mechanical nature of the process, where part properties are developed (evolve) simultaneously with the geometrical form of the part. This, combined with a poor process control, can often yield non-conformant process outcomes and part

defects. Such complex and highly non-linear systems often require heuristic-based approaches in conjunction with white-box physics-based models [5, 6]. One known such example is the stress-induced cracking of GFRP components during the de-moulding stage, compromising structural integrity of the part and perceived surface quality [4].

### 1.1 De-moulding process and its complexity

The de-moulding process in GFRP composite manufacturing is highly mechanical, where there is a need to apply external forces to the consolidated composite part, to remove it from the mould. Manufacturers may, e.g. use a multistep process to achieve this (Fig. 1) by (i) mechanically separating the oversprayed flanges of the part from the mould using soft plastic wedge, (ii) wedging an air-injection nozzle further between critical areas of the overspray flanges and striking the part with a cushioned tamper (to encourage the flow of air to separate a greater area of the two components) and finally (iii) a horizontal winch attached to embedded plywood sections in the composite part (which applies a displacement-controlled tensile force to separate it from the tool). The compressed air and wedges are not always able to fully separate the mould from the part, as the local forces become too small, and hence

✉ Abbas S. Milani  
abbas.milani@ubc.ca

<sup>1</sup> Composites Research Network-Okanagan Laboratory, School of Engineering, University of British Columbia, Kelowna, Canada

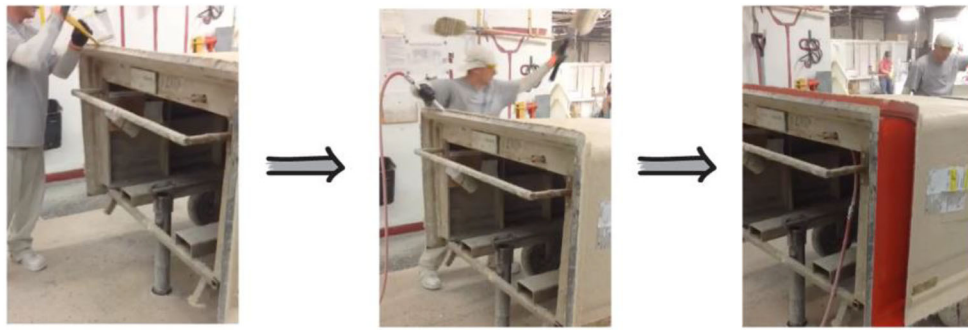


**Fig. 1** A typical three-stage de-moulding process of industrial size GFRP parts: (1) mechanically separating the overspray flanges of the part from the mould using a soft plastic wedge, (2) wedging an air-injection nozzle

further between the overspray flanges and striking the part with a cushioned tamper and (3) using a horizontal winch to separate the tool and part

the latter final stage of using the tensile force becomes necessary for successful removal of the part.

As a result of the large de-moulding forces placed upon the consolidated composite component, there is the potential for incurring damage. This is particularly the case in sharp corner radii areas, where the bending stresses are magnified [7] (see also Fig. 3 for an example). The purpose of the present case study is to use simulation and characterization tools and identify the root causes of corner cracking from process-based sources and recommend some general solutions to the designers, in order to assist in mitigating such cracking.

## 2 Case study

Manufacturers of GFRP composite shower stall units (Fig. 2) often use the spray-up method. This involves the deposition of a thin layer (normally in the range of 0.01–0.016") of unsaturated polyester-based gelcoat material (e.g. Maxguard LG-33LE-2270W) to give a white and glossy surface finish, as well as the deposition of both short, chopped fibres mixed with resin on to a tool, which forms the bulk laminate and shape of the final structure. For the gelcoat material, it is preheated by the spray gun nozzle to ~100 °F (38 °C) prior to ejection and deposition on the tooling surface, with the temperature of the surrounding (manufacturing shop) airflow

being uncontrolled and seasonally varying between 77 and 100 °F (25–38 °C). The gelcoat polymerization reaction is initiated, e.g. by the addition of Akzo Nobel ® C-50 Cadox Methyl Ethyl Ketone Peroxide (MEKP) initiator at a concentration ranging from 1.25 and 1.75% by volume, depending on the daily conditions. This initial layer is left for typically ~20 min to partially vitrify and have sufficient stiffness to support the following layers of material, while also being chemically active enough to provide further bonding. In the bulk laminate, the resin is chemically activated within the chop spray gun, with the addition of the necessary chemical agent(s). In the present case study, an unsaturated polyester (UPE) resin (Polylite 33010 UPE) is used with the same MEKP initiator as the gelcoat and at the same concentration, to begin the polymerization reaction. The resin has various filler materials added to it, for the purpose of modifying mechanical properties and lowering material cost. The E-glass fibres are chopped to a length of approximately 3 in. from a continuous roving and mixed with the aforementioned materials at the spray gun. Volume fractions of the constituent non-reinforcement materials in the resin at room temperature are 46% resin, 49.25% calcium carbonate filler, 4.05% Featherlite FL-4000 and 0.7% titanium dioxide. This distribution of materials is then combined with the fibreglass at a volume fraction of 12.5%. The nozzle of the gun preheats the mixed materials to 38 °C and is deposited on to the partially cured

**Fig. 2** The spray-up manufacturing process used to make GFRP shower stalls in the case study; (a) spraying gelcoat on to a prepared mould and (b) fibre/resin spray-up and roller consolidation of the bulk laminate



**Fig. 3** Example of a corner crack defect, seen in tub showers after de-moulding



gelcoat layer, the temperature of which can vary depending on a variety of parameters. Once the bulk laminate and stiffening core sections are fully deposited and co-cured, the part is ready to be de-moulded and undergo post-processing activities. This typically occurs after a target cure time of 60 min for the bulk laminate.

**2.1 Corner cracking**

For fibre-reinforced polymer composites (FRPCs), the de-moulding process is necessary to separate the consolidated part from the tooling used to form its shape. This process usually requires an external load be placed upon the tooling and part, in order to mechanically separate the two. This load is not insignificant, as the chemical and electrostatic bonding

between the tool and part can be large, even when surface preparation of the tooling prior to material deposition and cure has been performed. The load induces stresses within the part and can sometimes lead to local failure within the coated GFRP laminate material (Fig. 3). This is especially problematic for concave parts manufactured on a male tool, where it is difficult to provide extra reinforcement to the structure while de-moulding takes place. As such, excessive deflection can occur within the part, especially since the stiffness of the tooling is usually significantly higher than that of the part, so the latter effectively provides all deformation needed to separate the two surfaces.

The process is highly variable and dependent on the actions of the human operator. However, in this case study, the operators had in excess of 10 years of experience performing these

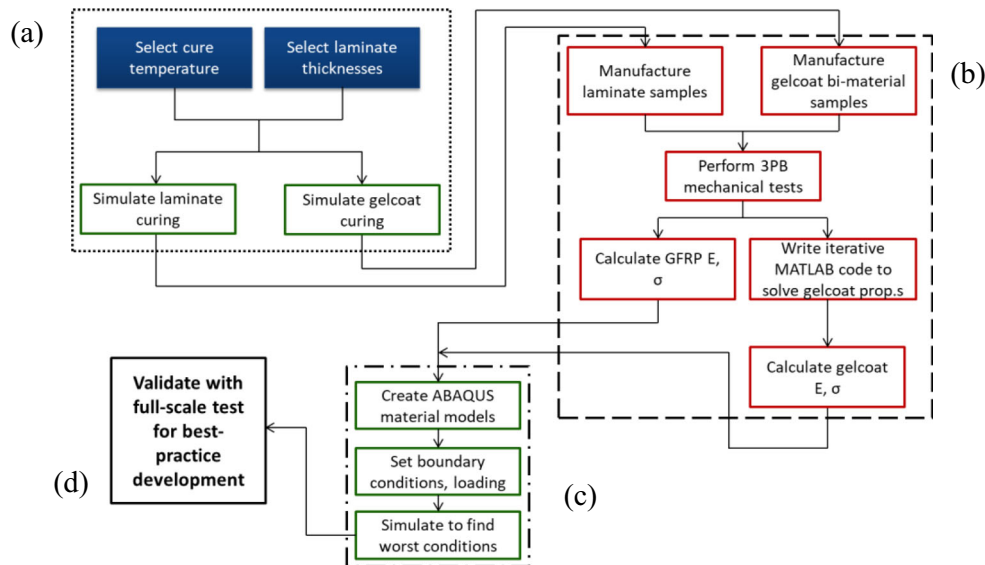
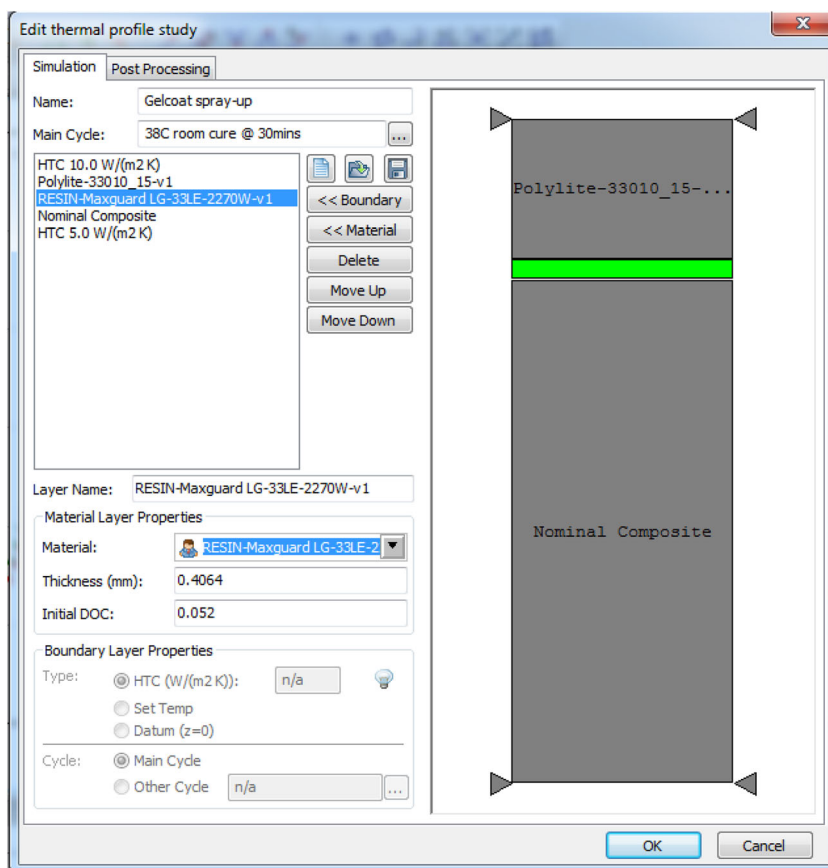


**Fig. 4** Workflow/best practice followed to investigate the corner cracking issue. Here, the process begins with determining the relevant material and processing conditions, as well as constructing a numerical cure simulation to determine degrees of cure (a dotted line), followed by mechanical testing of both GFRP laminate and gelcoat under the corresponding cure conditions to determine the associated mechanical properties (b

long-dashed line), then incorporated into a 3D structural simulation of the de-moulding process to assess which conditions result in cracking or no cracking (c dot-dash line), finally yielding a process map as a recommended safe operating envelope for the manufacturer and full-scale validation testing of the model (d solid line)

**Fig. 5** Graphical user interface of the model in RAVEN, used to run numerical model of the GFRP laminate and gelcoat cure process. Here, the material models are combined with the configured laminate and tool geometries, as well as the thermal boundary conditions, to perform the simulation. Degree of cure as a function of time is extracted from the model, for selected regions of the material



tasks. In previous internal studies performed by the company, it was concluded that the highly skilled operators responsible for this task were likely not a contributing factor in the generation of defects in this particular case.

## 2.2 Analysis procedure

It is recognized that there is a highly variable rate of corner crack defects among different composite manufacturing sectors, which can significantly reduce the efficiency of the overall manufacturing process and quality of final parts. Under nominal conditions, in the setting of this industrial case study, the defect rate can be typically 5%, yet in some instances, this has increased to as much as 25%. It was hypothesised that the development of composite mechanical properties during part cure would be the main driver for corner cracks, and this formed the basis for the modelling in this section.

Figure 4 shows the workflow used to investigate the occurrence of corner cracks. Based on initial engineering judgement, it was believed that two major factors of the underlying phenomenon are cure temperature and laminate thickness of the composite part. By selecting realistic bounds for these factors, it was possible to use cure simulation tools to evaluate the range of degree of cure (DOC) for the gelcoat and bulk

laminate materials. By correlating this with mechanical tests performed on laminate samples at different degrees of cure, a predictive model was developed to relate DOC to mechanical properties. As such, a variety of de-moulding scenarios were simulated, to investigate the development of stresses and cracks in the bathtub part, along with sensitivities between the selected process inputs (laminate thickness, cure temperature) and design outputs (laminate modulus and ultimate tensile strength).

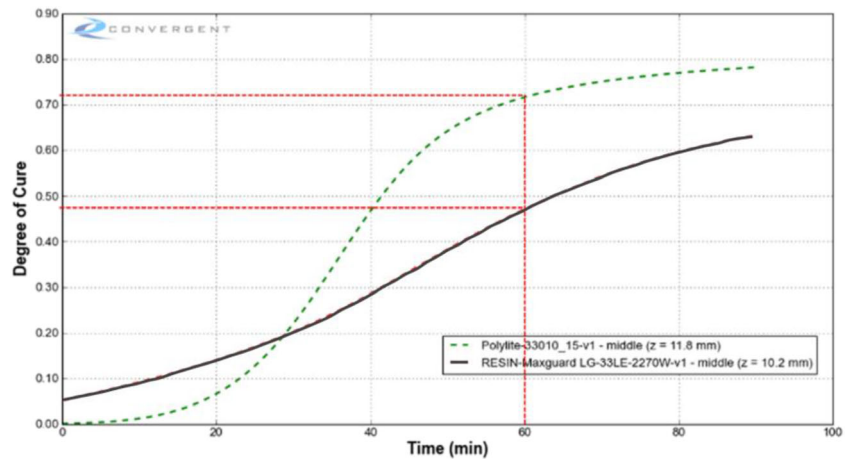
Following phase/box (a) in Fig. 4, the next section (Section 2.2.1) details the methods used to select the range of curing temperatures and material thicknesses for the gelcoat and bulk laminates, which were then needed to be used for performing numerical cure simulations (here in RAVEN®)

**Table 1** Summary of the obtained DOCs for the four different processing conditions, for both the gelcoat and bulk laminate

	Cold cure (25 °C)	Hot cure (38 °C)
Thin laminate (2.7 mm)	Gelcoat: 47%	Gelcoat: 83%
	Bulk laminate: 72%	Bulk laminate: 91%
Thick laminate (4 mm)	Gelcoat: 55%	Gelcoat: 87%
	Bulk laminate: 77%	Bulk laminate: 93%



**Fig. 6** Simulated cure response for gelcoat cure for the thin gelcoat ( $0.01''$  or  $2.45 \times 10^{-4}\text{m}$ ) and cold workshop ( $77^\circ\text{F}$  or  $25^\circ\text{C}$ ) temperature history



where the degree of cure under each configuration is determined (Section 2.2.2). Following, with the degree of cure estimated using the numerical tool, Section 2.2.2 covers the mechanical testing of both GFRP laminates and gelcoat-aluminium bi-material beams, to determine the bending modulus and strength of these materials, at the given manufacturing conditions (i.e. towards box (b) in Fig. 4). This includes describing how the gelcoat mechanical properties are numerically decomposed from the global properties of the bi-material beams. Further, Section 2.2.3 describes the structural finite element modelling of the GFRP part undergoing demoulding, using the relevant material property, load and boundary condition inputs, via a 3D model in Abaqus® (i.e. box (c)). Here, the combination of material thicknesses and cure temperatures is structurally assessed, to determine which configurations result in peak stress that will in turn cause cracking. Finally, Section 2.3 covers the creation of a process map that empirically captures the combination of material thicknesses and cure temperatures, as a recommendation to the manufacturer for a safer process operating envelope. This is also validated with a full-scale test in the manufacturing plant (i.e. box (d) in Fig. 4).

### 2.2.1 Process characterization and cure simulation

As previously stated, the two major processing factors influencing the development of corner cracks are deemed to be the laminate thickness and processing temperature. During the cure process, both of these parameters influence the bulk stiffness of the structure. This investigation required a simple 1D thermal analysis tool with cure kinetic modelling capabilities, to observe how the laminate degree of cure develops during the manufacturing cycle (as per part (a) in Fig. 4). The RAVEN software [8] was employed for this purpose. A simplified (1D) approach was used, as through-thickness heat transfer is the dominant mechanism of thermal transport in composite laminates of typical thickness [9]. In the manufacturing process, the deposition of the gelcoat material, preheated to  $100^\circ\text{F}$  ( $38^\circ\text{C}$ ), begins the cure process. This was modelled for two separate conditions; thin ( $0.01''$  or  $2.45 \times 10^{-4}\text{m}$ ) gelcoat, cold ( $77^\circ\text{F}$  or  $25^\circ\text{C}$ ) workshop air temperature, and thick ( $0.016''$  or  $4.06 \times 10^{-4}\text{m}$ ) gelcoat, hot ( $100^\circ\text{F}$  or  $38^\circ\text{C}$ ) workshop air temperature. These values were all within manufacturing tolerances, yet represented the allowable extremes. The two pairings were chosen, as thin laminates

**Fig. 7** Simulated cure response for gelcoat cure for the thick gelcoat ( $0.016''$  or  $4.06 \times 10^{-4}\text{m}$ ) and hot workshop ( $77^\circ\text{F}$  or  $25^\circ\text{C}$ ) temperature history

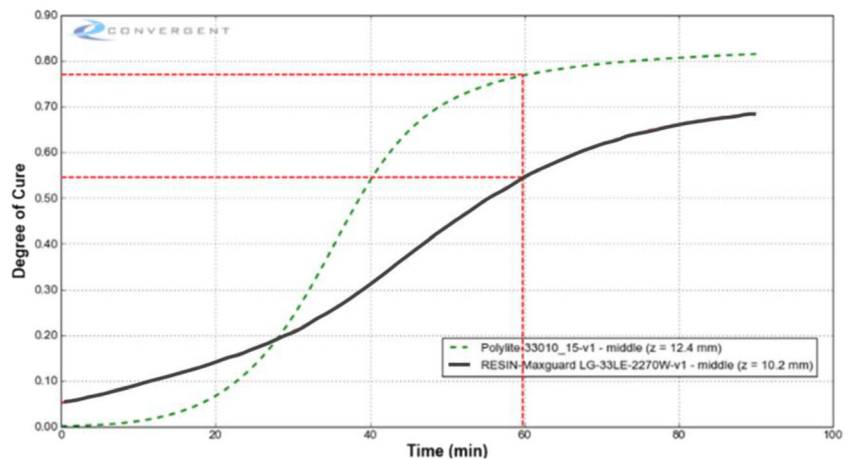
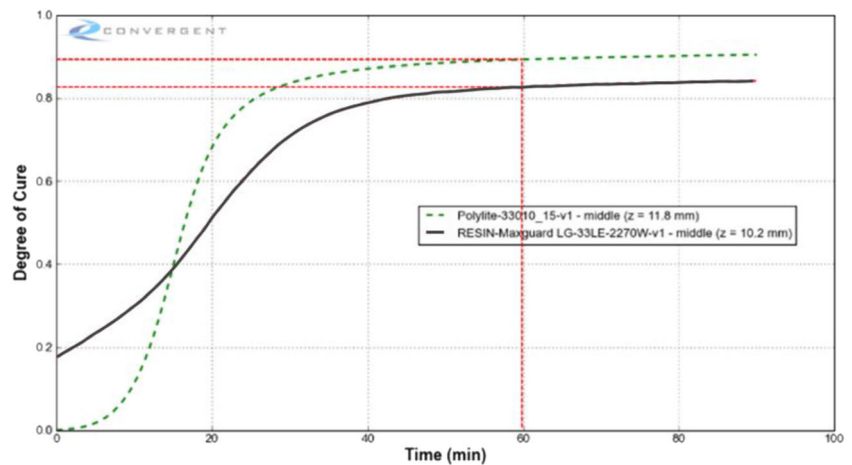


**Fig. 8** Simulated cure response for gelcoat cure for the thin gelcoat ( $0.01''$  or  $2.45 \times 10^{-4}$  m) and hot workshop ( $100^\circ\text{F}$  or  $38^\circ\text{C}$ ) temperature history



have a lower exotherm capability and combined with a cold air temperature, leading to a low temperature and low degree of cure case. The inverse applies to the condition of thick laminate and hot air temperature. Another important modelling parameter in the system definition is the heat transfer coefficient at the part and mould surfaces, responsible for the transfer of thermal energy between the system and its surroundings. The 1D model of the system has been shown in Fig. 5. A value of  $10 \text{ W/m}^2\text{K}$  was selected for the part surface, with higher air velocity due to its open nature and the structure often being in close proximity to the plant's HVAC system. For the mould underside,  $5 \text{ W/m}^2\text{K}$  was used, as the air is expected to be much more stagnant in that region. These values were selected based upon engineering judgement and with comparisons with other case studies that bear significant resemblances.

The fibre (12.5%) and filler volume fractions were included in the material model, to properly scale internal heat generation from the resin cure reaction, the thermal conductivity, diffusivity and specific heat capacities of the constituents, hence properly modelling the development, retention and flow of heat. The cure kinetics of the resin was previously

characterized using a modulated differential scanning calorimeter (DSC) as part of a separate study [10]. As per manufacturing specifications, the gelcoat layer was left to cure for 20 min prior to deposition of the next layer. This action typically occurs within a  $\pm 1$ -min interval. The output degree of cure and temperature at this time for each of the four conditions was recorded from the RAVEN model, which was then used as inputs for the gelcoat layer component of the system definition post-spray-up. Hence, as the bulk laminate layer underwent its exothermic chemical reaction, it could heat itself and the gelcoat layer further, providing insulation for the latter. Figure 5 provides a visual example of the RAVEN software and the construction of 1D layers in the numerical model.

#### Results of the cure simulation: effect of process factors

Figures 6, 7, 8 and 9 show the obtained model outputs for degree of cure (DOC) for the gelcoat layer and for the bulk laminate plus gelcoat. The initial gelcoat DOC was determined by a separate simulation step beforehand and used as an initial condition. The target de-moulding time for the bulk laminate was 60 min after deposition, which has been marked

**Fig. 9** Simulated cure response for gelcoat cure for the thick gelcoat ( $0.016''$  or  $4.06 \times 10^{-4}$  m) and hot workshop ( $100^\circ\text{F}$  or  $38^\circ\text{C}$ ) temperature history

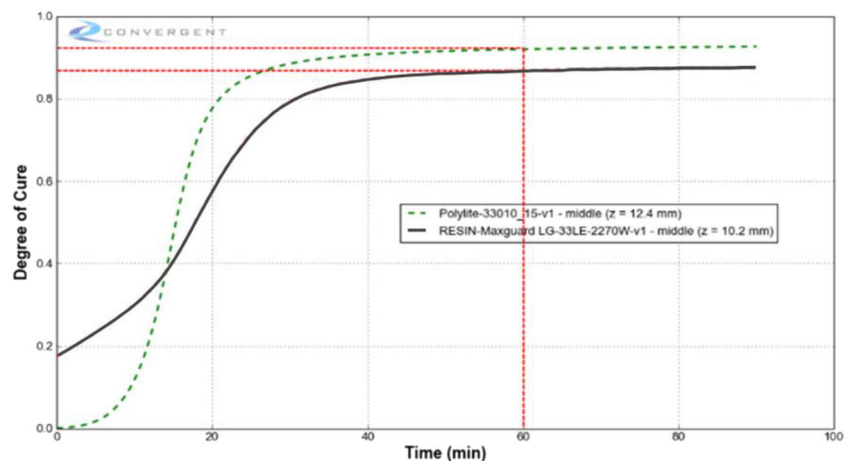


**Table 2** Results of mechanical property characterization for partially and fully cured bulk laminates

	Partially cured (DOC = 55%)	Fully cured (DOC = 98%)
Modulus of elasticity (GPa)	$E_{ave} = 3.882$ $E_{STD} = 0.589$	$E_{ave} = 5.448$ $E_{STD} = 0.644$
Ultimate bending strength (MPa)	$\sigma_{ave} = 61.362$ $\sigma_{STD} = 8.162$	$\sigma_{ave} = 70.748$ $\sigma_{STD} = 10.264$

on the curves. Following completion of the four process simulation conditions (Figs. 5, 6, 7 and 8), the degrees of cure were noted at the given de-moulding time and tabulated in Table 1. The previously presumed trends on thin/cold laminate leading to a low degree of cure and a thick/hot laminate leading to a high degree of cure held true via the RAVEN runs, per results in Table 1.

### 2.2.2 Test coupon fabrication and characterization of mechanical properties

Having collected the process simulation results, it was next necessary to tie these different degree-of-cure conditions to how the material properties develop throughout the cure cycle. For both the bulk laminate and gelcoat, experimental samples were prepared with degrees of cure approximately reflecting those obtained from the process simulation. Both materials were deposited on to lab-scale flat moulds, at the industrial manufacturing site, using their exact production material configuration. The samples were then placed into an ice-filled cooler with the appropriate physical protection, to avoid contamination and to stop the advancement of cure. Three-point bending (3PB) samples, adhering to ASTM D790 [11], were then cut using an abrasive waterjet cutter (AWJ). The 3PB condition was selected for testing, as it reflects the loading condition for the laminate when it is de-moulded in full scale. These samples were then cured in an environmental control chamber to match the process simulation cure results and finally tested under 3PB immediately. A total of five specimens were tested for each condition of the bulk laminate, for

statistical repeatability. From the load-displacement data obtained from a universal testing frame with 50 kN-load cell and extensometer, examples of the stress-strain responses are plotted in Figs. 10 and 11. The degrees of cure of the 3PB samples were determined using the same process simulation methodology in RAVEN, based upon the temperature history of the parts, from their manufacture, preparation and testing. These results have been included in Table 2. The obtained values were then applied to a scaling function to approximate the modulus at other DOCs (Fig. 12), where the scaling function is a bounded S-curve that captures the phase transition-based change in mechanical properties [12]; please see Appendix for more fundamentals on this transition.

Next, the same process was followed to determine the DOC and mechanical properties of the gelcoat film material. This process was more complex than the bulk laminate tests, as the gelcoat could not be de-moulded and tested independently. Hence, the gelcoat was cured on an aluminium 5052 mould, with a thickness of 0.05" or  $1.27 \times 10^{-3}$  m, and when the samples were cut, the aluminium was kept together with the gelcoat to make a bi-material beam for 3PB testing. Figure 13 shows the end-of-test condition of the two bi-material samples (partially and fully cured), as well as the corresponding stress-strain curves.

The modulus and strength directly extracted from the experiment are only effective values, as they are the sum of two components (aluminium and gelcoat) with their own moduli and geometries. Equation (1) [13] describes the effective stiffness of the bi-material test beam as a function of the

**Fig. 10** Stress-strain behaviour of the bulk laminate 3PB samples for the partially cured samples

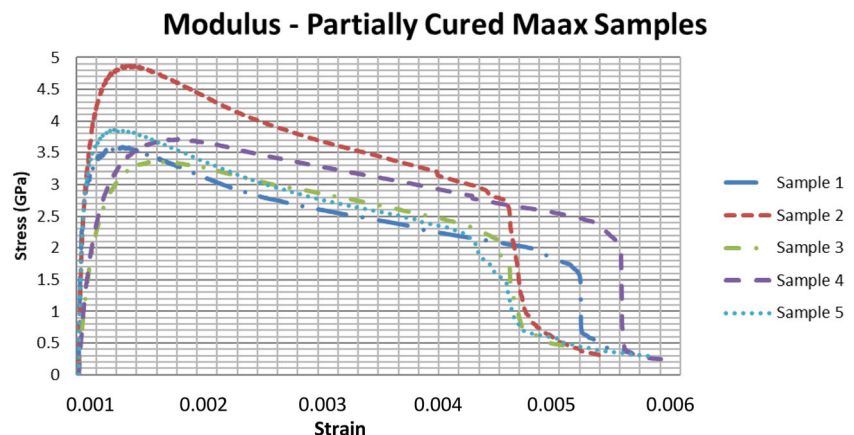
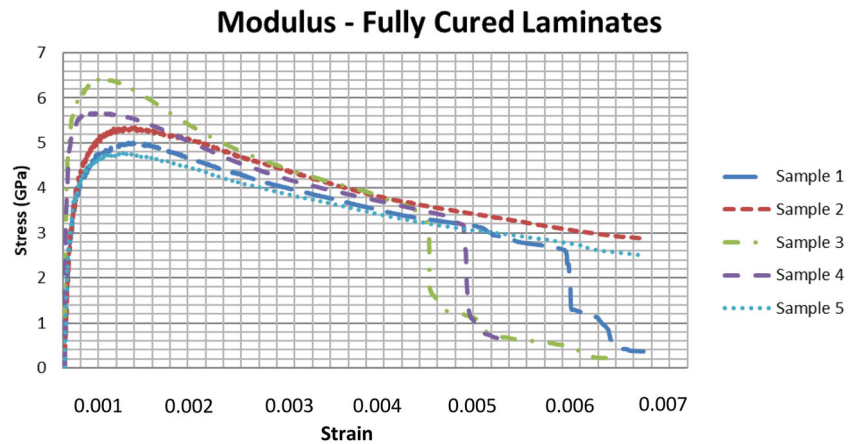


**Fig. 11** Stress-strain behaviour of the bulk laminate 3 PB samples for the fully cured samples



component materials and geometries. By iteratively solving for  $E_c$ , the modulus of the gelcoat can be isolated.

$$(EI)_{Eff} = \frac{w \cdot t_{st}^3 \cdot t_c \cdot E_{st} \cdot E_c}{12(t_{st} E_{st} + t_c E_c)} \left( 4 + 6 \frac{t_c}{t_{st}} + 4 \left( \frac{t_c}{t_{st}} \right)^2 + \frac{E_c}{E_{st}} \left( \frac{t_c}{t_{st}} \right)^3 + \frac{E_c t_c}{E_{st} t_{st}} \right) \quad (1)$$

where  $t_{st}$  and  $E_{st}$  are the thickness ( $m$ ) and modulus (Pa) of the substrate metallic layer respectively,  $t_c$  ( $m$ ) and  $E_c$  (Pa) are the thickness and modulus of the gelcoat layer, respectively, and  $w$  ( $m$ ) is the width of the bi-material beam.

The same previous methodology of using the scaling function to approximately calculate the modulus for a given degree of cure was used for the gelcoat (Table 3), and the estimated values were compared with a similar gelcoat from the literature (namely, Scott Bader Crystic 44PA). The similarity in mechanical properties provided more confidence in the performed experimental characterization using the bi-material beam method [13].

#### Elastic Modulus

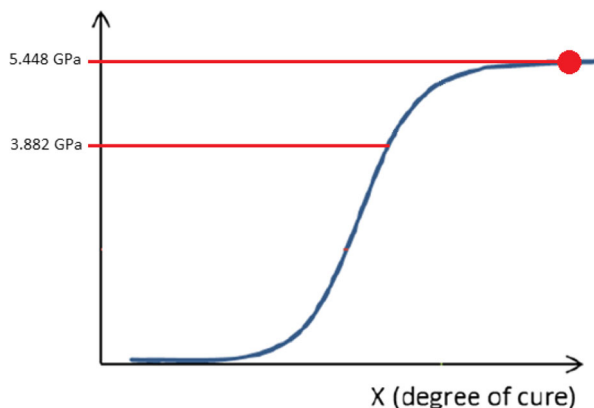


**Fig. 12** Fitting the experimental points on to a scaling function; relating the laminate elastic modulus and degree of cure. The S-curve scaling function is typical for polymer-matrix composites, representing the transition from liquid to crystalline phase [12]

#### 2.2.3 Structural simulation of the de-moulding

In order to effectively reduce the rate of corner crack occurrence in the open-moulded GFRP part, it was eventually necessary to investigate how stresses in the corner locations develop under different processing and design conditions. To this end, a 3D structural finite element model was developed to incorporate different material properties (cure/temperature dependent), part thicknesses as well as de-moulding boundary conditions and evaluate the influence of these three factors on the development of the stresses. Next to material properties in Tables 2 and 3, for the sake of a realistic numerical analysis, a representative part was first cured in the manufacturer shop on a mould of similar geometry to an actual bathtub product and de-moulded with a load cell attached, i.e. with the maximum load experienced during the actual process being recorded. The part was cured on its mould with typical mould preparation procedures applied to it beforehand and was then de-moulded at approximately  $45^\circ$  orientation. It was de-moulded with no assistance from compressed air or mechanical wedging, such that the full bonding characteristics could be investigated. The representative part was approximately rectangular in shape with dimensions of  $72'' \times 36''$  and when de-moulded with an overhead crane had a peak load of 1180 N, equating to an approximate bonding strength of  $705.6 \text{ N/m}^2$ . This value was then used in the subsequent numerical analysis, as the bonding strength between part and mould needed to be overcome for a successful de-moulding action. It is worth noting that for a shape as complex as a tub shower, the coupling factor between the mould and part depends on the loading conditions very much. For example, a surface being de-moulded in shear mode would have a different net force for de-moulding compared with surfaces that are perpendicular to the de-moulding load; i.e. in tension mode.

As boundary condition, a 60PSI pressure was applied to the tub base and back wall (Fig. 14), originating from when the operators first attach shop air lines at that pressure to the drain and overflow sections of the tub shower. Next, the mould



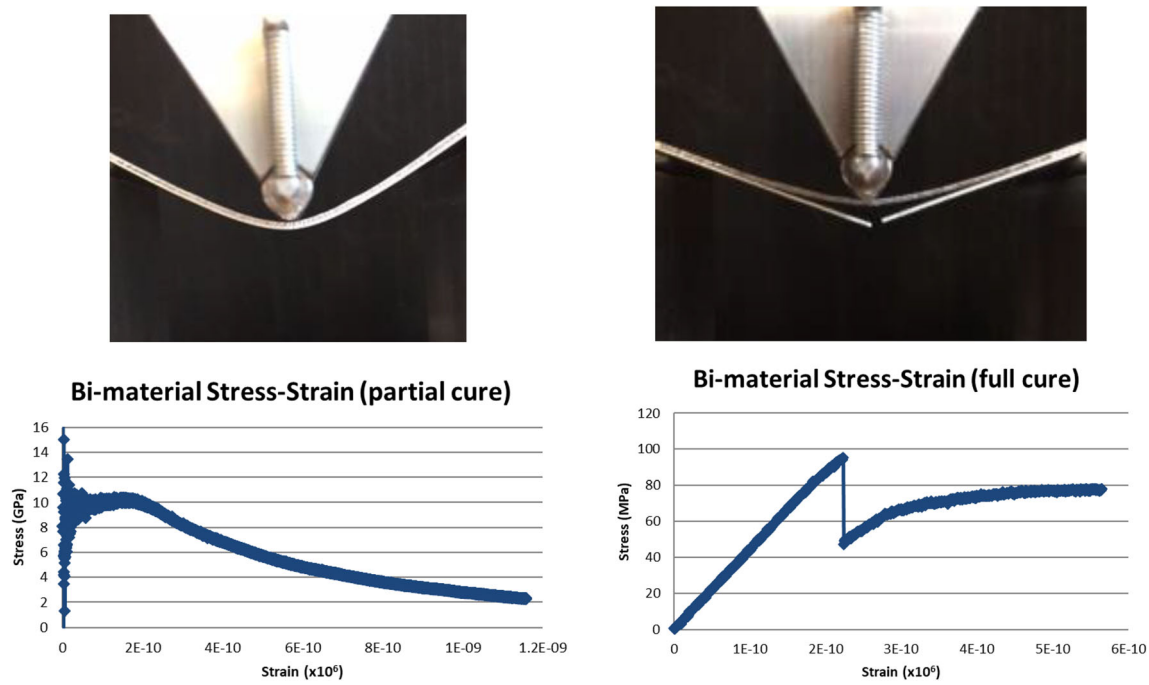


**Fig. 13** A visual example of the testing of two of the bi-material beams; (left) partially cured and (right) fully cured. Here, the partially cured condition results in highly plastic deformation, whereas the fully cured condition results in a brittle failure

segments around the periphery were disbonded one by one, as per the manufacturing procedure where a mechanical wedge is moved around the perimeter to de-mould the edge sections. Finally, an external load of 500 N was applied to the bottom-front section as a distributed load (approximately 6.11 ft<sup>2</sup> or 0.568 m<sup>2</sup>), simulating the final act of using a horizontal winch to de-mould the part completely, as depicted in Fig. 14.

For the stage where the fixed boundary conditions were sequentially removed, it was important to take into account that in practice, there are points where the moulds are likely to remain stuck to the parts. In most real de-moulding cases, only a few faces on the back wall remain stuck if the compressed air is not able to separate them (case 1). Conversely, a larger span of the back and side walls can remain fixed (case 2). In the latter case, this could be due to poor mould surface preparation prior to the manufacturing cycle. Figure 15 shows an illustrative case of these conditions (case 1: 100 °F cure, case 2: 77 °F cure, both laminates have 0.01" thickness), where the maximum stress is experienced in the bottom corner of the structure, which was in line with the actual location of the real cracking. Notice that due to overcured material condition associated with higher processing temperature, the maximum von Mises stress for case 1 is higher and hence higher risk of corner cracking.

### 2.3 Empirical optimization and in situ validation

Based on the developed material properties and stresses during the process, the next goal was to determine an appropriate de-moulding time to minimize the cracking. Conceptually, this optimum should be based on the material properties being partially developed and compliant enough during de-moulding (i.e. not to be too brittle and cause cracking due to the induced forces and moments), while also being stable enough such that substantial postcure after de-moulding does not occur, which is undesirable and can cause unrecoverable residual deformations [10, 15–22]. Determining this exact time point experimentally or analytically is complex and involves significant non-linear analysis [16]. Hence, an experience-based approach was opted herein. Namely, at a typical de-moulding time of 60 min, Eq. (2) was graphically applied to cure simulations to determine that the cure rate of the bulk laminate was approximately  $8 \times 10^{-5} \text{ s}^{-1}$  [15]. This was then used as a benchmark to be applied to other cases of workshop temperatures and laminate thicknesses, where the preferred de-moulding time would be when the cure rate of the laminate decreases below that threshold of  $8 \times 10^{-5} \text{ s}^{-1}$ . Figure 16 shows the plot generated from such empirical

**Table 3** Results of mechanical properties for partially and fully cured gelcoat layer

	Partial DOC (68%)	Full DOC (98%)	Crystic 44PA [14]
Modulus of elasticity (GPa)	5.45	6.5	5.2
Ultimate tensile strength (MPa)	Did not fail (120)	92.3	46

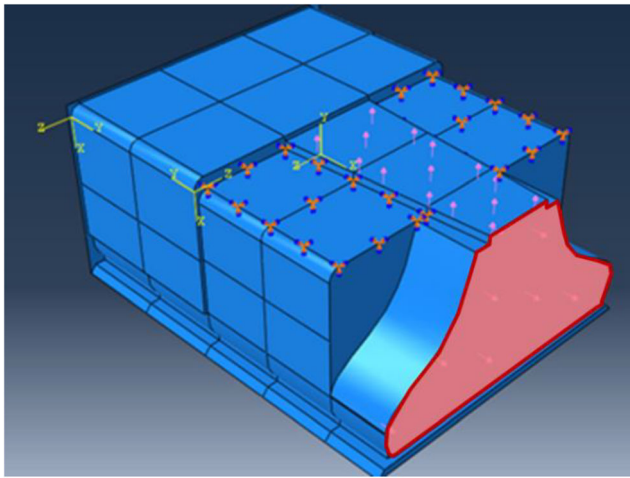


**Fig. 14** The region of the finite element model (light-shaded region) where the 500 N external load was applied to simulate the de-moulding process

approach, where de-moulding time is a function of the workshop temperature; the bands are given for the upper and lower limits for the cases of thick and thin laminates.

$$\frac{d\alpha}{dt} = \frac{K\alpha^m(1-\alpha)^n}{1 + e^{C\{\alpha - (\alpha_{C0} + \alpha_{CT}T)\}}} \quad (2)$$

$$K = Ae^{(-E/RT)} \quad (3)$$

where  $\alpha$  is the degree of cure,  $K$  describes the Arrhenius function for the reaction,  $\alpha_{C0}$  is the critical degree of cure at  $T = 0$  K,  $\alpha_{CT}$  is a constant accounting for increase in critical resin degree of cure with temperature and  $m$  and  $n$  are constants obtained from a curve-fitting analysis.

Subsequently, a follow-up in situ experiment was run at the manufacturing site, using results of the obtained empirical plot. For a workshop temperature of 90 °F, a de-moulding time of 40 min was selected and applied to the manufacturing cycle. This 40-min time was the mean value between the upper and lower bound estimates for acceptable de-moulding time, based on the structural simulation results. That is, given the

mechanical properties of the gelcoat and laminate that were experimentally determined for the given laminate thicknesses and air temperature, the structural simulation showed that any more or less time will result in poor mechanical properties and, hence, cracking of the structure. In the in situ validation experiment, no corner cracking was present, and feedback from the technicians indicated that the part stiffness was low enough to provide sufficient displacement during the de-moulding process.

### 3 Conclusion

This case study tackled a complex industrial manufacturing problem related to corner cracking during de-moulding of GFRP parts with 3D geometrical features. To this end, the cure processes of the GFRP laminate and gelcoat substrate layer were numerically simulated using RAVEN, based on typical material thickness and workshop temperature conditions. Following, experimental samples were manufactured with the associated degrees of cure, to determine the associated mechanical properties of bending modulus and bending strength. This was performed for monolithic GFRP laminates representing the product bulk laminate, as well as the gelcoat deposited on an aluminium sheet, forming a bi-material beam. In the case of the latter samples, the gelcoat mechanical properties had to be numerically decomposed from the net load-response curve of the combined materials. Further, a 3D structural simulation was formed using these material properties, combined with other process-specific load and boundary conditions, to explore the design space for feasible configurations of the model inputs of material thickness and workshop air temperature. By performing mechanical testing on a set of laminate materials (mimicking different processing conditions) and developing a structural FEA model with boundary and loading conditions reflecting the manufacturing practice, it was determined that boundary condition case 1 (only a few

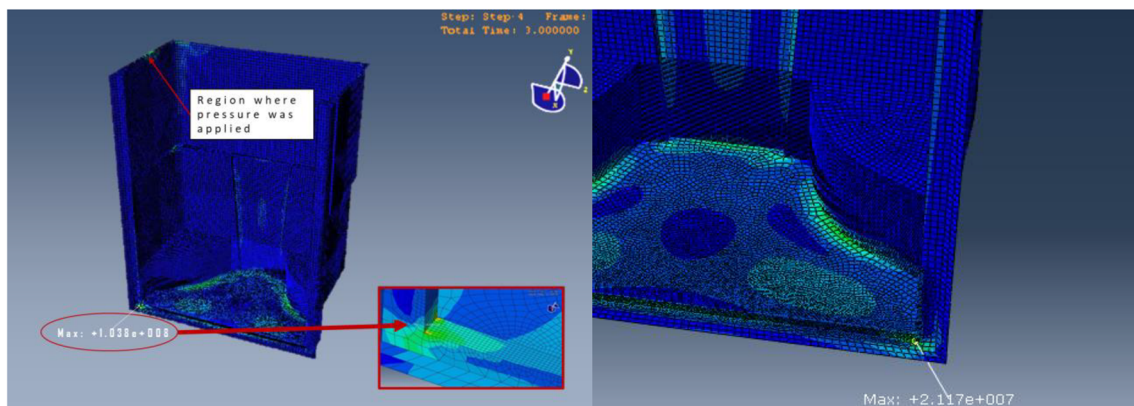


**Fig. 15** Structural simulation of the de-moulding process, showing the location of the maximum stresses developed in (left, maximum stress 103.8 MPa) case 1 and (right, maximum stress 21.2 MPa) case 2, agreeing with the real case (see also Fig. 3)

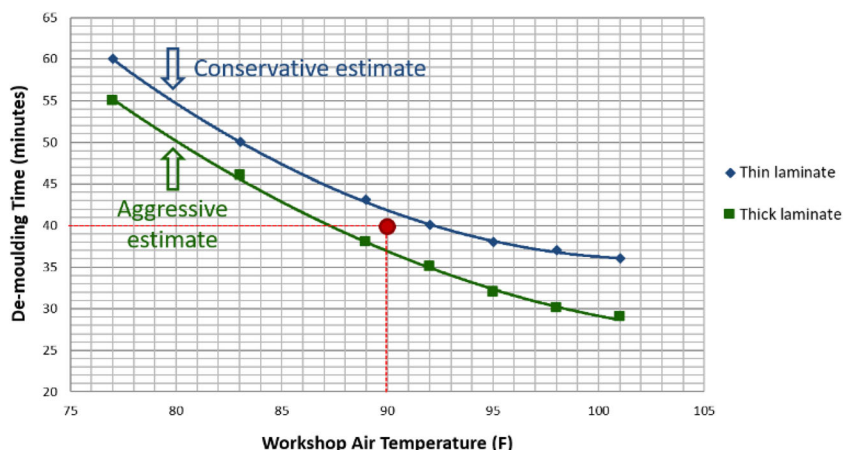


**Fig. 16** Best-practice process chart obtained to predict the de-moulding time of the GFRP part. This chart acts as guidance for manufacturer on de-moulding time, as a function of the laminate thickness and the workshop temperature. The green (lower) data series represents the lower threshold for acceptable de-moulding time. Conversely, the blue (upper) data series is for upper threshold estimates. Outside of these

bounds, the de-moulding process is likely to result in cracking of the GFRP product, based on the combined material properties and boundary/load conditions investigated in the finite element simulations. The red point represents an example point in the decision space, from the in situ validation test. That is, the workshop temperature was 90 °F, and the mean value between the upper and lower bounds for time is 40 min

faces on the back wall remain stuck where the compressed air is not able to separate them), higher material thickness and higher air temperature combination could yield the highest chance for the cracks to develop. When the process model was further refined to account for the development of material properties over cure time, a follow-up experiment was run at an industrial scale to give evidence that the final model is effective in reducing defect rates and potentially increasing process productivity towards lean manufacturing.

**Appendix: a closer look to the effect of resin curing**

The development of the resin modulus throughout the manufacturing process primarily influences the bulk mechanical properties of the composite laminate prior to de-moulding. Specifically, once the initiator compound is added to the resin mix, the generation of free radical particles begins and chemical bonding between monomers into long polymer chains begins, as depicted in Fig. 17.

As the chains grow longer with more monomers added, the overall mobility of the molecules diminishes, and bulk rigidity becomes higher. This leads to an eventual transition from a liquid into a solid state, which becomes glassy as the available mobility effectively reduces to zero. Similarly, as this progresses, so does the measurable modulus of the material. Figure 18 shows both an example relationship between a cure temperature, degree of cure and glass transition temperature of an unsaturated polyester resin and the generic relationship between degree of cure and developed elastic modulus.

It is important to note that the cure process is dependent on not only temperature but also time, as the chemical reaction has many factors that make the timescale great enough for de-moulding activities to take place during material property changes. The development of cure and hence material properties can be modelled in many ways, typically done empirically using a differential scanning calorimeter (DSC) and then curve-fitting the results to an assumed phenomenological model. There are many that have been developed for particular material systems, each with their own mechanics. For a

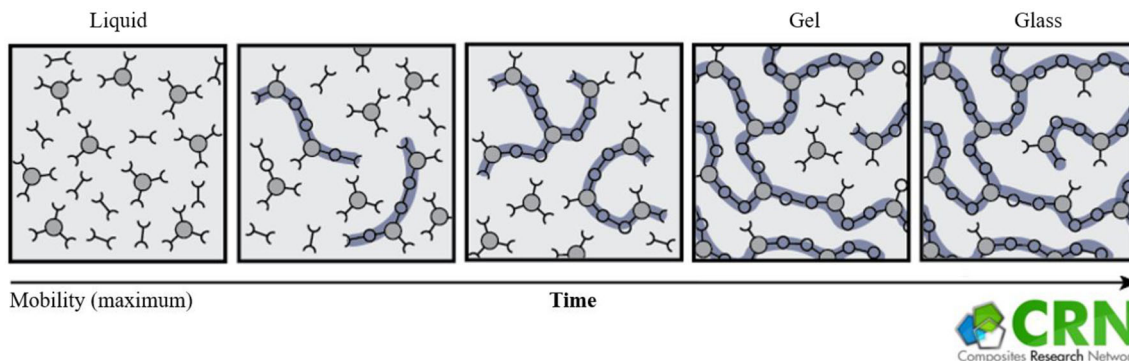


**Fig. 17** Illustration of how resin modulus develops due to lower molecular mobility as the cure cycle progresses



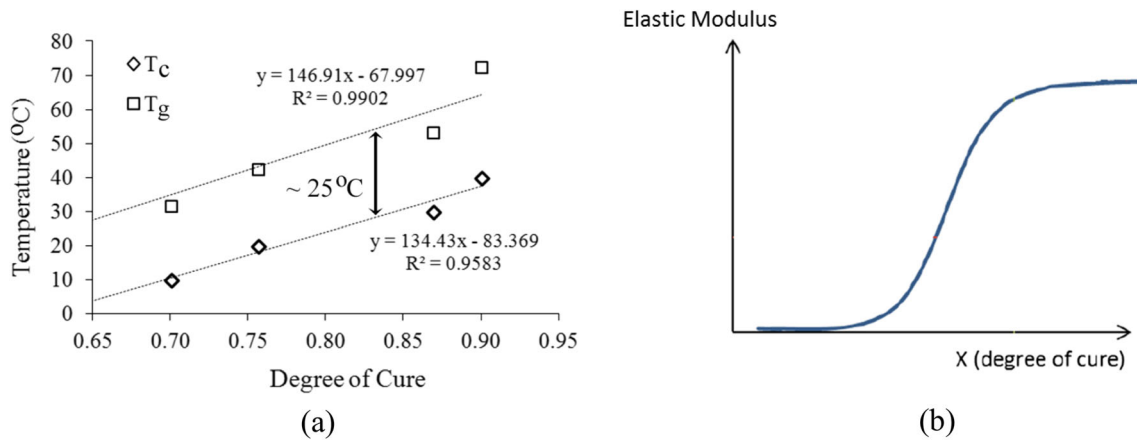


**Fig. 18** (a) Example of a cure temperature ( $T_c$ ), degree of cure and glass transition temperature ( $T_g$ ) relationship for an unsaturated polyester resin [19], (b) the generic relationship assumed between degree of cure and elastic modulus [19]

chemical system with a heavy dependence on diffusion-based mechanisms, Cole et al. [20] developed Eq. (4) shown below, which has been effective in other published works [19].

$$\frac{d\alpha}{dt} = \frac{K\alpha^m(1-\alpha)^n}{1 + e^{C\{\alpha - (\alpha_{c0} + \alpha_{cT})\}}} \quad (4)$$

$$K = Ae^{(-E/RT)} \quad (5)$$

where  $\alpha$  is the degree of cure,  $K$  describes the Arrhenius function for the reaction,  $\alpha_{c0}$  is the critical degree of cure at  $T = 0$  K,  $\alpha_{cT}$  is a constant accounting for increase in critical resin degree of cure with temperature and  $m$  and  $n$  are constants obtained from a curve-fitting analysis.

## References

- Strong BA (2008) Fundamentals of composites manufacturing: materials, methods and applications, 2nd edn. Society of Manufacturing Engineers, Dearborn
- Robert IM (2001) Fibre Reinforced Polymers – From Aerospace to Infrastructure, ATSE Focus, No. 107
- Cunningham J (2015) The difficulty of qualifying exotic materials and processes for flight. Engineering Materials. <http://www.materialsforengineering.co.uk>. Accessed 06 Mar 2020
- Mazumdar SK (2002) Composites manufacturing, materials, product and process engineering, 2nd edn. CRC Press, Boca Raton
- Khan MA, Kumar AS, Poomari A (2012) A hybrid algorithm to optimize cutting parameter for machining GFRP composite using alumina cutting tools. Intl J Adv Manuf Tech 59:1047–1056
- Huang Y, Liu S, Xiao G, He Y, Wang W (2020) Experimental investigation into the effects of adhesion wear on belt grinding of glass fiber reinforced plastics. Intl J Adv Manuf Tech 109:463–473
- Torres J (2015) Effect of geometrical and process parameters on the quality of open moulded composite parts with sharp corners: a decision-based approach. Dissertation, University of British Columbia
- Convergent Manufacturing Technologies Inc. (2020) RAVEN Simulation Software. <https://www.convergent.ca/products/raven-simulation-software>. Accessed 20 Apr 2020
- Shimizu T, Kotlik JC, Arafath ARA, Poursartip A (2008) Evaluation of temperature profiles in thick composite parts during autoclave processing. Proceedings of 23rd ASC Technical Conference:1–17
- Shah Mohammadi M, Solnickova L, Crawford B, Komeili M, Milani AS (2014) Investigating the unrecovered displacement of glass fibre reinforced polymers due to manufacturing conditions. J Multifunctional Compos 2:100–104
- Guidelines for property testing of composites. In: CMH-17 Composite Materials Handbook – Revision G Volume 1. SAE International, Wichita, pp 82–203
- Baran I, Cinar K, Ersoy N, Akkerman R, Hattel J (2017) A review on the mechanical modeling of composite manufacturing processes. Arch Comput Methods Eng 24:365–395
- Thorpe R (2013) Experimental characterization of the viscoelastic behavior of a curing epoxy matrix composite from pre-gelation to full cure. Dissertation, University of British Columbia
- Scott Bader (2020) Crystic gelcoat 44PA – sandable spray gelcoat. [https://www.scottbader.com/wp-content/uploads/4006\\_crystic-gelcoat-44pa-gelcoat-en-feb13.pdf](https://www.scottbader.com/wp-content/uploads/4006_crystic-gelcoat-44pa-gelcoat-en-feb13.pdf). Accessed 15 Apr 2020
- Fernlund G, Floyd A, McKay S (2007) Process analysis and tool compensation for curved composite L-angles. Proceedings of the 6th international conference on composite materials (ICCM)
- Fernlund G, Floyd A, Shewfelt M, Hudek M (2007) Process analysis and tool compensation for a complex composite panel. In proceedings of the 6th international conference on composite materials (ICCM)
- Twigg G (2001) Tool-part interaction in composites processing. Dissertation, University of British Columbia
- White S, Hahn H (1993) Cure cycle optimization for the reduction of processing-induced residual stresses in composite materials. J Compos Mater 27(14):1352–1378
- Bogetti TA, Gillespie JW (1992) Process-induced stress and deformation in thick-section thermoset composite laminates. J Compos Mater 26(5):626–660
- Cole KC, Hechler JJ, Noël D (1991) A new approach to modeling the cure kinetics of epoxy/amine thermosetting resins. 2. Application to a typical system based on bis[4-(diglycidylamino)phenyl]methane and bis(4-aminophenyl) sulfone. Macromolecules 24(11):3027–3468



21. Fernlund G, Poursartip A, Twigg G, Albert C (2003) Residual stress, spring-in and warpage in autoclaved composite parts. Proceedings of the 4th international conference on composite materials (ICCM)
22. Zhao L, Warrior N, Long A (2007) A thermo-viscoelastic analysis of process-induced residual stress in fiber-reinforced polymer-matrix composites. Mater Sci Eng A 452:483–498

**Publisher's note** Springer Nature remains neutral with regard to jurisdictional claims in published maps and institutional affiliations.

Reproduced with permission of copyright owner. Further reproduction prohibited without permission.